DD

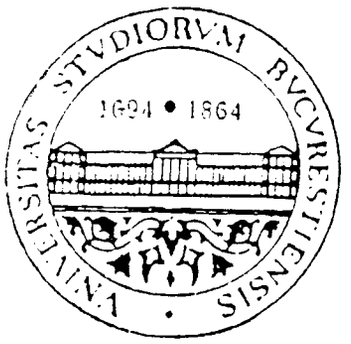

BUCHAREST UNIVERSITY

EXPERIMENTAL PARTICLE PHYSICS GROUP

UBPub. EPPG/Phys. 30
March 1996

Electron Microstrip Silicon Detector for High Flux Density

D. Dascalu[1], C. Gingu[1], D. Liviu[1], T. Angelescu[2], A. Mihul[2], A. Vasilescu[3]

[1] *Institute of Microtechnology, Erou Iancu Nicolae 34B, P.O.Box36-160, Bucharest, Romania, Fax: +40-1-3124661*
[2] *Physics Department, Bucharest University, P.O.Box MG-12, Bucharest, Romania, E-mail: tangel@roifa.ifa.ro*
[3] *Institute of Nuclear Physics and Engineering, P.O.Box MG-6, Bucharest, Romania, E-mail: angela@roifa.ifa.ro*

Abstract

The possibility to use a silicon microstrip detector in hypernuclei electroproduction studies is examined. The high electron flux density (10^7e/cm^{2}s) on the detector induces surface damage: a change of about 10 V in the flatband voltage and an increase of the leakage current. Bulk damage is negligible. A simulation of charge collection showed that for a read-out capacitance 10 times the interstrip capacitance and an interstrip capacitance 10 times the strip-to-ground capacitance we can collect the charge every 4 strips with 90% efficiency. A 50 μm strip pitch and a 200 μm read-out pitch ensure an 80 μm spatial resolution for tracks inclined at 30 degrees and 160 μm for tracks inclined at 60 degrees. The signal-to-noise ratio of 15 before irradiations decreases due to the increase of the leakage current up to 5, still sufficient for a high detection efficiency.

Electron Microstrip Silicon Detector for High Flux Density

D. Dascălu[1], C. Gangu[1], D. Livin[1], T. Angelescu[2], A. Mihul[2], A. Vasilescu[3]

[1] *Institute for Microtechnology, Bucharest, Romania, POBox 36-160, Fax: +40-1-3124661*
[2] *Physics Department, Bucharest University, P.O.Box MG-12, Bucharest, Romania,*
e-mail: tangel@roifa.ifa.ro
[3] *Institute of Nuclear Physics and Engineering, P.O.Box MG-6, Bucharest, Romania,*
e-mail: angela@roifa.ifa.ro

Abstract

The possibility to use a silicon microstrip detector in hypernuclei electroproduction studies is examinated. The high electron flux density (10^7e/cm^{2}s) on the detector induces surface damage: a change of about 10 V in the flatband voltage and an increase of the leakage current. Bulk damage is negligible. A simulation of charge collection showed that for a read-out capacitance 10 times the interstrip capacitance and an interstrip capacitance 10 times the strip-to-ground capacitance we can collect the charge every 4 strips with 90% efficiency. A 50 μm strip pitch and a 200 μm read-out pitch ensure an 80 μm spatial resolution for tracks inclined at 30 degrees and 160 μm for tracks inclined at 60 degrees. The signal-to-noise ratio of 15.5 before irradiations decreases due to the increase of the leakage current up to 5, still sufficient for a high detection efficiency.

1 Introduction

Electroproduction of hypernuclei at the Continuous Electron Beam Facility (Virginia, U.S.A.) benefits of high current and duty factor , and a very high precision in the beam energy, providing information on interaction potentials in manybody hadronic systems.[1]

The experiment approved at CEBAF studies the ^{12}C(e,e'K$^+$)$^{12}_{\Lambda}$B reaction using a two arm spectrometer for the detection in coincidence of the scattered electron and produced kaon.

Fig. 1 gives the top view of the spectrometer layout.

The missing mass ($^{12}_{\Lambda}$B energy states) resolution is limited by the beam resolution and the kaon arm momentum resolution to about 200 keV. The split pole magnet (Fig. 2) in the electron arm spectrometer gives a resolution of about 150 keV/mm in the focal plane; using a MPWC for electron detection in the focal plane with 0.5 mm spatial resolution we obtain for the electron arm a momentum resolution which does not alter the overall missing mass resolution.

In the further step of the experiment a beam dispersion is foreseen which will give a ten times better resolution. In these conditions the MPWC is no more adequate. The focal plane electron detector should have a spatial resolution of 100 μm or less, giving thus a small contribution, of only 25 keV, to the missing mass resolution.

The present paper studies the possibility of using a silicon microstrip detector in the electron focal plane and establishes its designing conditions.

2 Geometrical Conditions

The split pole focal plane shown in Fig. 2 is 74 cm long and 2.5 mm wide. The focal plane has a very small curvature (sagitta ~40 μm) which will not be taken into consideration in designing the detector.

Electrons are falling on the focal plane at an angle of 36-60 degrees, so the tracks are inclined in the detector.

The detector should have ten aligned sensors, 7 cm long and 4 cm wide, with vertical strips on one side. The electronics can be placed above or below the detector.

3 Radiation Damage

The focal surface (7·40×2.5 mm^2) is hit by 2×10^8 e/s (i.e. the flux density is about 10^7 e/cm^{2}s).

Electrons in the momentum range 240 375 MeV/c are minimum ionising particles (mip). They deposit in the detector a dose of 8.7 kGy for 600 h of beam time. Ionisation induces surface damage in the detector by creating electron-hole pairs in the oxide layer; holes are trapped in the oxide and increase the fixed positive charge a at the SiO_2 Si interface. Consequently the flatband voltage is increasing. The depletion voltage should be higher in order to compensate for the flatband voltage change. The results of Wunstorf *et al.*[2] showed that the flatband voltage increases with about 10 V for doses around 30 kGy and saturates at this value. The accumulation layer at the SiO_2 Si interface affects the interstrip capacitance and interstrip resistance. Before irradiation interstrip resistances are typically about 10 GΩ and saturate at full depletion. After irradiation they fall by 2 3 orders of magnitude and no longer saturate at the depletion voltage. This effect is accompanied by an increase in surface leakage current (up to 2 μA/cm^2 at 50 kGy [2]). Biased detectors have a leakage surface current 4 times higher, but it disappears in about one hour [3]. Interstrip capacitance is increasing up to 10 kGy and remains constant for higher doses. There is no clear difference between biased and unbiased detectors [4].

The bulk damage in detectors irradiated with high energy electrons has been investigated experimentally by Dale *et al.*[5]. Evaluations of A. van Ginneken [6] are shown in Fig. 3. At 300MeV/c the electron NIEL curve reaches a plateau 20 times lower than that of the protons. The electron fluence for 600 h of beam time is 2.16×10^{13}e/cm^2. For this fluence we do not expect type inversion and the total depletion voltage does not change very much, the bias voltage can be kept in normal limits. Using the liniar dependence of the damage constant (α) with NIEL we obtain for the electron bulk damage leakage current 60 μA/cm^2 (18 nA/strip).

Due to the trapping of the charges the current pulse induced by the free electron hole pairs created inside the depleted volume will have a larger tail when increasing the fluence. For a short collection time (20 40 ns) the charge collection will be incomplete. The charge deficit for electrons should be negligible due to the much smaller bulk damage [7].

In conclusion the bulk damage is small compared to the surface damage, which should be taken into consideration when chosing the processing technology.

4 Silicon microstrip detector design

The severe radiation damage conditions involve attentive examination of different detector designs. We describe some characteristics of the L3-SMD [8]. One ladder of this detector has the requested dimensions for the CEBAF experiment. The ohmic side strips are implanted every 50 μm. p$^+$ blocking strips designed to interrupt the accumulated surface charge between the n$^+$ strips alternate with n$^+$ strips. The read-out pitch is 200 microns. Strips are biased through guard ring as shown in fig. 4.

The read-out strips are capacitively coupled to SVX-II chips, glued on each module. Each channel has a low noise amplifier with a gain of about 19 mA/fC. [9] The read-out capacitance (150 pF) is much larger than the interstrip capacitance C_s=1.3 pF/cm, condition necessary for a complete charge collection. (see section 6)

The chips are glued and bonded to an aluminum nitride substrate. The hibrid circuits dissipate heat which should be elliminated by cooling the detector. The read-out electronics consists of charge sensitive preamplifiers, an auxiliary electronic board, an analog-to-digital converter and an optical transmission line to the data acquisition system.

4.1 Read-out channels, multiplicity factor and kapton routing variants

The ten silicon sensors are aligned on the base plate, using 3 precise pin positioning for each wafer. The wafers are glued on the base plate, which supports also the electronics and the water cooling pipes.

One silicon sensor contains 1409 strips at 50 μm pitch. Read-out at 200 μm allows the use of 353 read-out strips per sensor. The total number of read-out strips is 3530 and they will be Viking type. Six variants of multiplicity factor and kapton routing have been analysed. The right variant should optimise at least the following criteria:

- the capacitance of the multiplied strips for a read-out channel should be low
- the number of Viking chips and hibrids should be low
- the average inclined lines pitch on multiplicity kapton should be larger than 50 μm.

Table 1 summarises the principal characteristics of the six variants. According to the above criteria, we will probably use variant V3. The corresponding drawing is presented in fig. 9.

5 Spatial Resolution

The spatial resolution is related to different characteristics of the sensor: the strip pitch, the read-out pitch, as well as to the track inclination to the sensor plane, the multiple scattering, the magnetic field effect, the detector alignment.

With a cluster finding method we can investigate the influence of these factors on the precision in finding the cluster which determines the spatial resolution of the sensor.

When traversing a detector, a particle at minimum ionisation creates a constant number of electron-hole pairs along its path. The charge is collected by the strips. The charge centroid gives the cluster position (the track intersection with the sensor) and the residue distribution with respect to the reconstructed track in other aligned detectors permits the evaluation of the spatial resolution.

The number of strips collecting charge (the cluster window N_w) is given by: $N_w = 2 + 1.1t\tan\alpha/p$ where t is the thickness of the silicon wafer , p is the pitch of the read-out strip.[11]

The cluster window is chosen to be the number of consecutive strips, where the sum of collected charges were greater than $1.5\sigma_{sum}$ ($\sigma^2_{sum} = N_w\sigma_i^2$).

σ_i is found from the pedestal. The pedestal is the average of ADC counts in each channel and σ_i is the r.m.s. of pedestals.

Thus we find $Q_i = ADC^i - P^i_{ed}$. With the charge weighted average of the coordinates of the strips in the cluster window the centroid is:

$$< y^{AC} >= \frac{\sum y_i Q_i}{\sum Q_i}$$

The cluster width is a function of the incidence angle of the track on the detector. For 30° the cluster width is about 4 read-out strips.

The spatial resolution has been determined by aligning the studied detector along the test beam, with two reference detectors and two scintillators in coincidence. The r.m.s. of the clusters with respect to the reconstruction track in the reference detectors define the spatial resolution of the studied sensor.

For tracks perpendicular to the detector the spatial resolution is given by $p/\sqrt{12}$ (60 μm for 200 μm pitch) [10]. For 200 μm read-out pitch the resolution varies between 80 μm at 30° inclination of the track to the detector surface , up to 160 μm at 60 degrees.[11]

Variant number	V1	V2	V3	V4	V5	V6
Strip multiplicity	5	5	4	3	3	2
Kapton pcs. multipl.	4	2	2	2	2	2
Kapton pcs. fan-out	1	1	1	1	2	2
Kapton dim. multipl.(cm)	28.8x3.5	36x3.5	36x3.5	36x3.5	36x3.5	36x3.5
Kapton dim. fan-out (cm)	14.4x3.5	14.4x3.5	18x4.1	24x5.3	12x3.5	18x4.1
Lines/kapton pc. multipl.	706	1412	1323	1176	1176	882
Lines/kapton pc. fan-out	706	706	882	1176	588	882
Average inclined lines pitch on multiplicity kapton(μm)	48	89	74	57	103	74
Total read-out channels	706	706	882	1176	1176	1764
Total Viking chips	6	6	7	10	10	14
Total hibrids	1	1	1	2	2	2
Estim.capacitance of one read-out channel	$5C_s$+59.3C_k	$5C_s$+32C_k	$4C_s$+29C_k	$3C_s$+25C_k	$3C_s$+13.9C_k	$2C_s$+9.6C_k

Table 1: Principal characteristics of multiplicity factor and kapton options

n	k	Q_L/Q_k	Q_R/Q_k	$(Q_L+Q_R)/Q_k$
5	2	0.624	0.100	0.724
	3	0.345	0.345	0.690
	4	0.999	0.624	0.724
10	2	0.707	0.019	0.726
	3	0.512	0.064	0.576
	4	0.368	0.116	0.484
	5	0.261	0.179	0.440
	6	0.179	0.261	0.440
	7	0.116	0.368	0.484
	8	0.064	0.512	0.576
	9	0.019	0.707	0.726

Table 2: Results of simulations for C_s=10, C_g=1 and C_R=100, for different n and k values

6 Simulation of Charge Division in Silicon Microstrip Sensors

6.1 Capacitive Charge Division Principle

One possibility to improve the spatial resolution of Si microstrip sensors is to take advantage of the capacitive charge division principle.

Consider a microstrip detector with a geometrical strip pitch p_{st}. The read-out electronics read the strip charge of each n_r-th strip. Thus the read-out pitch p is $n_r p_{st}$. If C_s is the interstrip capacitance, C_g the strip to ground capacitance and C_R the read-out electronics capacitance, then the microstrip sensor can be represented by the capacitive network from fig. 5.

If the particle is passing somewhere between two read-out strips, the charge generated is collected by the nearest strip (or strips, for inclined tracks). Then a fraction of the generated charge is arriving at the two neighbouring read-out strips through the capacitive network. The fraction of the read-out charge is higher if the ground capacitance (C_g) is lower and the read-out capacitance (C_R) is higher: $C_g << C_s << C_R$ [12]. The position of the incident particle can be further computed from the charge collected at the left and right read-out strips (Q_L and Q_R), using different position finding algorithms.

6.2 Mathematical Approach

In our following analysis we are considering only the capacitive network between two adjacent read-out strips, as shown in the scheme in fig. 6. This approximation is consistent with the practical requirements.[12] We will consider that in the node k a charge Q_k is generated by a passing particle. Our purpose is to compute the charges Q_L and Q_R as a function of network parameters: C_s, C_g, C_R, n and k. Applying the charge conservation law, we solved the following system of equations (1):

$$\begin{aligned}
cV_1 - aV_2 &= 0 \\
-aV_1 + bV_2 - aV_3 &= 0 \\
&\vdots \\
-aV_{k-1} + bV_k - aV_{k+1} &= Q_k \\
&\vdots \\
-aV_{n-2} + bV_{n-1} - aV_n &= 0 \\
-aV_{n-1} + cV_n &= 0
\end{aligned}$$

where

$$\begin{aligned}
a &= C_s \\
b &= 2C_s + C_g \\
c &= C_g + C_R
\end{aligned}$$

After finding the potentials V_1, ... V_n, the left and right read-out charges can be easily calculated as (2)

$$\begin{aligned}
Q_L &= cV_1 \\
Q_R &= cV_n
\end{aligned}$$

6.3 Simulation Results

Simulations were made for different values of capacitance (C_s, C_g, C_R), read out pitch (n) and charge generation position (k). An example is shown in Table 2, for C_s=10, C_g=1 and C_R=100, for different values of n and k. The values of the collected left and right charges as well as the sum variation can be readily seen.

We have also obtained the variation of the collected charge for different values of C_s, C_g and C_R. One important result is the Q_L/Q_k and Q_R/Q_k are dependent only on the ratios C_s/C_g and C_R/C_s, being independent of the absolute values of the capacitances.

The ratio

$$\frac{C_g}{C_s} = \frac{\ln(p_{st}/w_{st})}{\ln(4t^2/p_{st}w_{st})}$$

where w_{st} is the strip width and t the sensor thickness.[12]

For example Fig. 7 shows the respective $(Q_L+Q_R)/Q_1$ variation for n=5 and k=3 as a function of C_g/C_s, with C_s/C_R as a parameter.

The simulation results can also be applied to the case of inclined tracks. In this case we must calculate first the number of intermediate strips between which the particle passes.(I_{st}=[N_u] 2, where N_u is given in section 4, and [x] represents the integer part of x.)

The charge per strip Q_{st} is

$$Q_{st} = \frac{Q_{tot}}{I_{st}}$$

with Q_{tot} the total charge deposited by the inclined passing particle.

Since the system (1) is linear, using the superposition principle, the solution for inclined tracks will be the sum of individual solutions of the system (2), for the I_{st} with Q_{st} corresponding to Q_k, Q_{k+1}, ...,$Q_{k+I_{st}-1}$.

7 Signal-to-Noise Ratio and Detection Efficiency

Both signal and noise are measured in ADC counts which can be converted into equivalent number of electrons using the average number of electron-hole pairs created in silicon by a mip.

The ADC signal has a Landau distribution (fig. 8). For the SMD L3 detector [13] the Landau distribution parameters are Q_{MP}=43.2 ADC and Γ_{Landau}=(4.3±0.24) ADC, (1 ADC=600 e).

The noise in the detector is due to fluctuations in the bulk and surface currents and the read-out electronics. For the same detector the average noise was 2.5 ADC before irradiation. Thus the signal-to-noise ratio was S/N=15.5.

We evaluated the leakage current after irradiation to be about 38 nA/strip. This corresponds to 4900 e collected in a 20 ns collection time. After irradiation S/N=5.

Signals are registered if S/N≥3 for the given channel. If this condition is fulfilled, all signals with S>15 ADC are registered. On the Landau distribution cited above the detection efficiency is 97.3%.

8 Conclusions

A silicon microstrip detector 74 cm long and 4 cm wide with one side strips of 50 μm pitch and 200 μm read-out pitch is designed for electron detection in a hypernuclei electroproduction experiment. The spatial resolution expected is about 150 μm for tracks inclined at 30 ÷ 60 degrees. The charge collection simulation shows that for capacitances fulfilling the condition C_R : C_s : C_g=10/1/0.1 we collect about

90% of the deposited charge. Signal-to-noise is about 15.5 before irradiation and diminishes to 5 after 600 h of beam time due to the leakage current induced by the high electron fluence.

The detection efficiency is not altered by this effect.

References

[1] *Investigation of the spin dependence of the ΛN effective interaction in the p shell*, CEBAF Note EXP 89-009

[2] R. Wunstorf *et al*, *Damage induced surface effects in silicon detectors*, presented at the 7th Symp. Semic. Det., Elmau (1995)

[3] C. Leroy *et al*, CERN/ECP 93-12, (1993)

[4] A. Holmes Siedle *et al*, NIM A339 (1994) 511

[5] C. J. Dale *et al*, IEEE Trans. Nucl. Sci., NS-35(6), 1208, (1988)

[6] A. van Ginneken, Fermi Nat. Lab Note FN-522, (1989)

[7] A. Boden *et al*, NIM A340 (1994) 491

[8] M. Acciari *at al*, CERN PPE/94-122
R. Battiston *et al.*, NIM A 334 (1994) 216

[9] S. Kleinfelder, IEEE Trans. Nucl. Sci. NS-35 (1988) 171

[10] S. J. Bates *The effects of proton and neutron irradiations on silicon detectors for the LHC*, RALT-006 (1993)

[11] H. Hanai, KEK preprint 91-175, OULNS 91-09

[12] J.B.A. England *et al*, NIM A185 (1981) 43

[13] A. Adam *et al*, NIM A344 (1994) 521

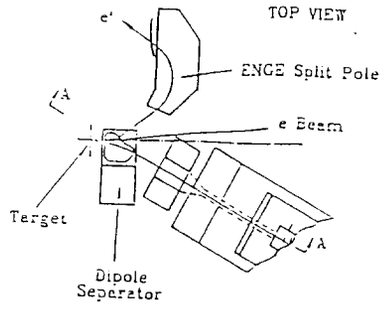

Fig. 1. Top view of the spectrometer layout for (e,e'K+) reaction

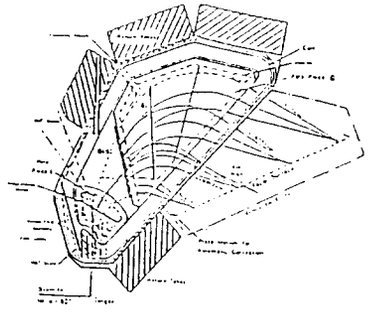

Fig. 2. A layout of the split pole spectrometer

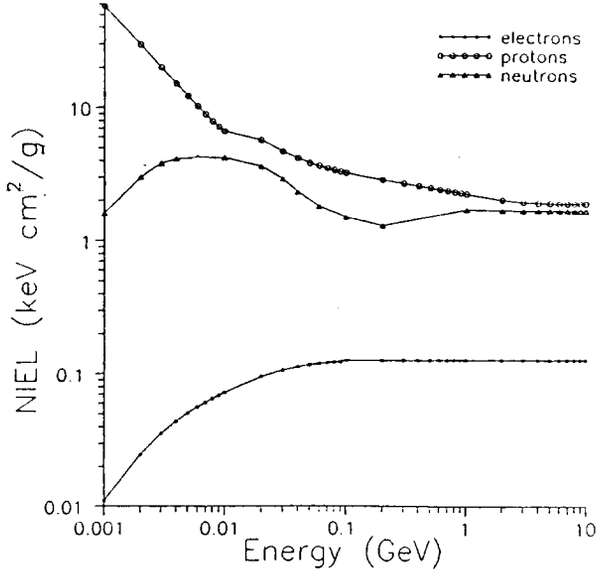

Fig. 3. Non Ionising Energy Loss versus incident energy

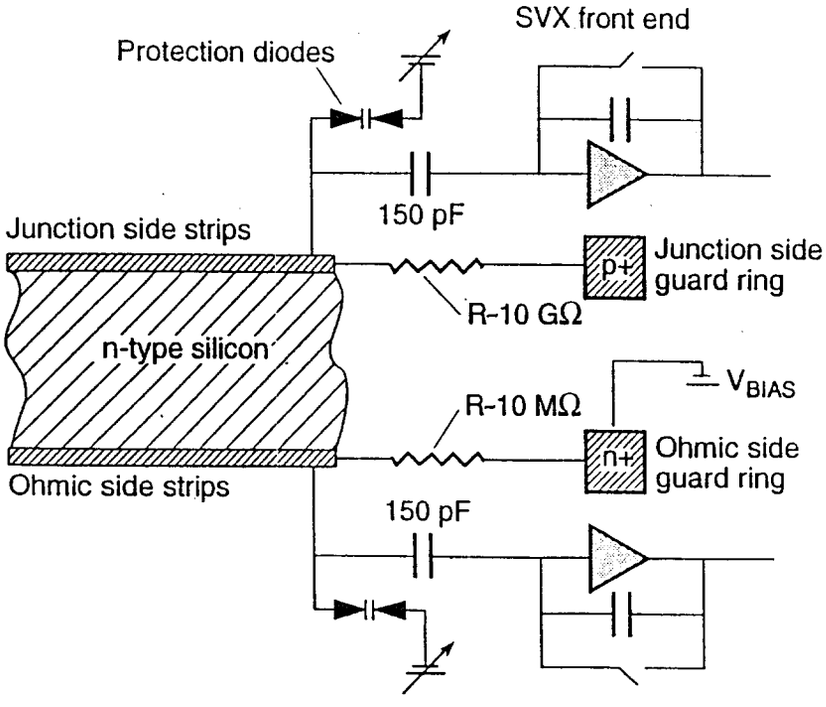

Fig. 4. Equivalent circuit for the biased SMD sensor

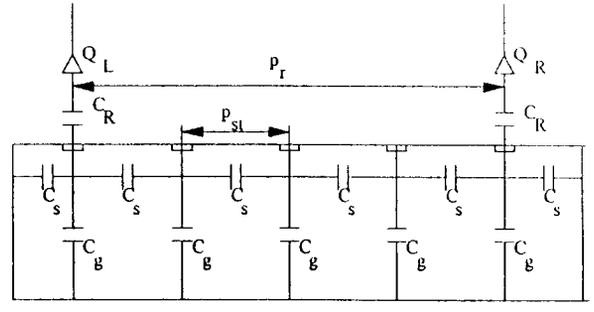

Fig. 5 Capacitive network of a Si microstrip sensor with connected read-out electronics

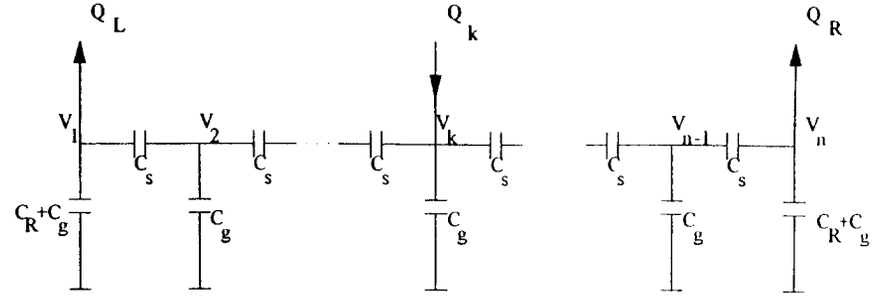

Fig. 6 Scheme of the capacitive network

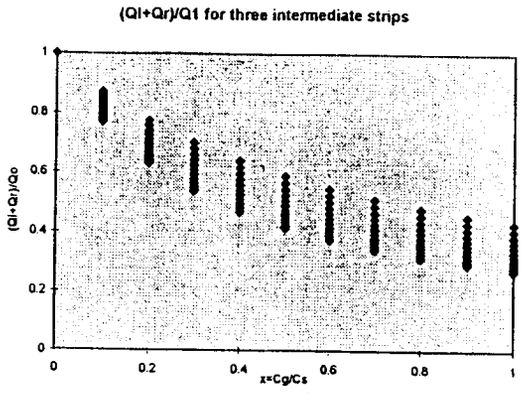

Fig. 7. $(Q_L+Q_R)/Q_1$ variation versus C_g/C_s for n=5, k=3 and $C_s/C_R=0\div1$

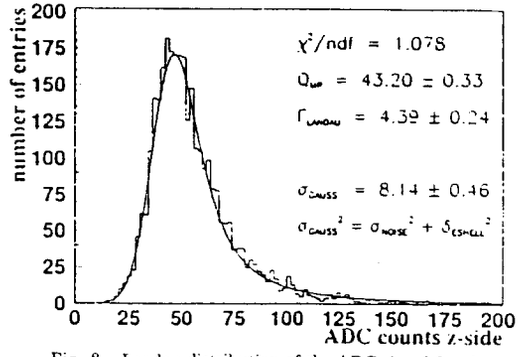

Fig. 8. Landau distribution of the ADC signal for the z side of the SMD-L3 detector[13]

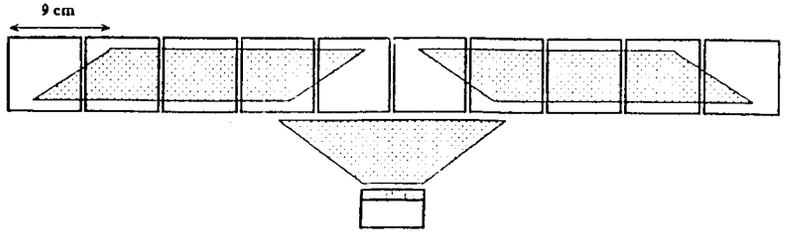

Fig. 9 Kapton routing for variant V3